Inorganic Chemistry

Article

pubs.acs.org/IC

pH- and Dopant-Dependent $CdMoO_4$:Mn Nanocrystals: Luminescence and Magnetic Properties

Qilin Dai,[†] Gongguo Zhang,[‡] Pan Liu,[†] Jing Wang,[‡] and Jinke Tang*[,†]

[†]Department of Physics and Astronomy, University of Wyoming, Laramie, Wyoming 82071, United States

[‡]Ministry of Education Key Laboratory of Bioinorganic and Synthetic Chemistry, State Key Laboratory of Optoelectronic Materials and Technologies, KLGHEI of Environment and Energy Chemistry, School of Chemistry and Chemical Engineering, Sun Yat-sen University, Guangzhou, 510275, China

ABSTRACT: $CdMoO_4$:Mn nanocrystals with a tetragonal crystal structure were prepared by aqueous coprecipitation method at a low temperature of 2 °C under different pH values. The size of the $CdMoO_4$:Mn nanocrystals of spherical morphology increases with the Mn dopant concentration from 35 to 55 nm for pH = 4. The morphology could be tuned from nanocrystals to microstructures consisting of smaller nanoparticles by the Mn concentration when the pH value of the precursor was increased to 8. The thermal stability of the luminescence and magnetic properties of the Mn-doped samples also depend on the pH and the doping level. The effects of the pH and dopant on the luminescence and magnetic properties, including magnetic susceptibility and electron paramagnetic resonance, were investigated. This approach contributes to better understanding of aqueous chemistry methods to control the growth of nanocrystals.

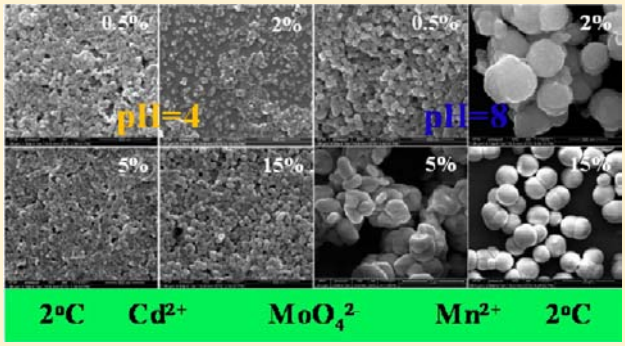

1. INTRODUCTION

As important materials in the optics and opto-electronics industry, metal molybdates have been intensively studied over the past few years due to their potential applications in photoluminescence, optical fibers, and scintillators.[1−4] Among them, cadmium molybdate ($CdMoO_4$), isostructural to $CaMoO_4$ and $PbMoO_4$, is an interesting wide bandgap semiconductor with scheelite structure. $CdMoO_4$ exhibits several unique properties, for example, electronic excitation with VUV synchrotron radiation,[5] pressure-induced phase transformations,[6] and interesting spin−lattice relaxation.[7]The properties of nanosized materials are attracting current interest. They are important not only for applications but also for gaining essential understanding of nanocrystals, the quantum confinement effect, and surface effect, etc. Significant effort has been devoted to the synthesis of $CdMoO_4$ micro- and nanocrystals with aqueous methods, including $CdMoO_4$ nanoparticles prepared by hydrothermal process,[8] octahedral $CdMoO_4$ nanocrystals synthesized via a microemulsion-mediated route,[9] and hollow $CdMoO_4$ structures obtained in aqueous solutions at room temperature.[10] However, only inhomogeneous nanoparticles or microsized particles composed of nanosized subunits were obtained. It is still a challenge to obtain uniformly dispersed nanocrystals because they have the tendency to aggregate. It is important to synthesize homogeneous $CdMoO_4$ nanocrystals to meet the demands of device applications.

pH is an important parameter in the wet chemistry synthesis particularly in aqueous synthesis to control the size, morphology, and structure of the nanocrystals. The effects of the pH value on the sample structure and properties have been investigated in different materials. Research has shown that pH can control the synthesis of Au nanocrystals so as to achieve blue, green, and red fluorescent emission,[11] tune the drug release related to mesoporous silica nanocomposite,[12] and change the size, morphology, and the structure to improve the photoluminescence.[13−16] The second parameter is temperature, which also can have great effects on the size and morphology of the nanocrystals. Usually, the size and aggregation of the nanocrystals are dependent on the growth rate of the nanocrystals in wet chemical synthesis, which is strongly correlated with the temperature of the growth environment. High temperature would increase the activity of the ions in the solution resulting in fast growth speed and leading to larger size and aggregation of the nanocrystals. Room temperature and hydrothermal conditions (120 °C) have been used to prepare $CdMoO_4$ of aggregated nanostructure.[8,10] There is no report on the synthesis of $CdMoO_4$ nanocrystals at lower temperatures to our knowledge. The third parameter is the dopant in the crystal lattice which would control the size and structure of the nanocrystals.[17−19] Recently Liu proposed that Gd^{3+} ion has strong effect on $NaYF_4$ crystal growth rate through surface

Received: March 30, 2012
Published: August 16, 2012

 © 2012 American Chemical Society dx.doi.org/10.1021/ic3006663 | *Inorg. Chem.* 2012, 51, 9232−9239

charge modification leading to tunable reduction of the size of the $NaYF_4$ nanocrystals.[17] Herein, Mn ions were chosen to dope into $CdMoO_4$ to control the size and morphology of the nanocrystals, which resulted in interesting magnetic properties as well. A coprecipitation method with different pH values at low temperature (2 °C) was developed to prepare Mn-doped $CdMoO_4$ nanocrystals of different size and morphology on a large scale. The photoluminescence and magnetic properties induced by the dopant were investigated as a function of the pH and Mn doping concentration. The results show that the pH value and Mn doping concentration have dramatic influence on the growth mechanism of $CdMoO_4$:Mn nanocrystals by controlling the Ostwald ripening process. The thermal stability of photoluminescence, ferromagnetic/antiferromagnetic exchange coupling, and electron paramagnetic resonance (EPR) spectra also vary with the pH value and Mn concentration.

2. EXPERIMENTAL SECTION

2.1. Synthesis of $CdMoO_4$:Mn nanoparticles. $CdMoO_4$:Mn nanoparticles were prepared by the reaction of $NaMoO_4{\cdot}2H_2O$ (Alfa Aesar, 98%), $Cd(OOCCH_3)_2{\cdot}2H_2O$ (Alfa Aesar 98%) and $Mn(OOCCH_3){\cdot}2H_2O$ (Alfa Aesar 96%) at low temperature. All chemicals were used as received without further purification. In a typical synthesis process, 9.95 mmol $Cd(OOCCH_3)_2{\cdot}2H_2O$, 0.05 mmol $Mn(OOCCH_3){\cdot}2H_2O$, and 10 mmol $NaMoO_4{\cdot}2H_2O$ were dissolved in 180, 20, 200 mL deionized water, respectively. Then the former two solutions were mixed together followed by the addition of Na_2MoO_4 solution with vigorous stirring. The pH value (pH = 4, 8) of the mixed solution was adjusted dropwise with CH_3COOH or NaOH solution. The concentrations of CH_3COOH and NaOH are 1 M and 2 M, respectively. After 30 min of magnetic stirring, the resulting suspension was stored in a refrigerator at 2 °C for 5 days without stirring or shaking. The resulting products were collected by centrifugation, washing several times with deionized water, and drying in vacuum overnight. Finally the powders of $CdMoO_4$:Mn were obtained. Samples of different Mn concentrations (0.5, 2, 5, and 15 mol %) were prepared by the same procedure except for changing the ratio of $Cd(OOCCH_3)_2{\cdot}2H_2O$ and $Mn(OOCCH_3){\cdot}2H_2O$.

2.2. Measurements. Powder X-ray diffraction (XRD) data were collected with a Philips X'Pert diffractometer using Cu Kα radiation. Scanning electron microscopy images were taken on a JEOL field-emission scanning electron microscope (FESEM) JEOL5800LV. Optical absorption was analyzed in a 1 cm cell in deionized water using a Cary 50 UV−vis spectrophotometer. The photoluminescence (PL) and photoluminescence excitation (PLE) spectra at room temperature were measured by FSP920 Time Resolved and Steady State Fluorescence Spectrometers (Edinburgh Instruments, UK) equipped with a 450-W Xe lamp, TM300 excitation monochromator and double TM300 emission monochromators, and red-sensitive PMT. The spectral resolution for the steady measurements is about 0.05 nm in UV−vis. For the temperature-dependent measurements, the samples were mounted in a 77−300 K Optistat DN-V liquid nitrogen optical cryostat with an ITC601 temperature controller (Oxford Instruments, UK). Magnetic data on 100−300 mg of powder samples of $CdMoO_4$:Mn were measured on a Physical Properties Measurement System (PPMS) from Quantum Design. DC magnetic susceptibility measurements were conducted between 5 and 300 K. The EPR spectra were recorded at room temperature using a Bruker ER041XG.

3. STRUCTURAL PROPERTIES

3.1. Crystal Structure and Morphology. The crystal structure of the $CdMoO_4$:Mn nanoparticles was characterized by XRD (Figure. 1). The XRD patterns for the $CdMoO_4$:Mn nanoparticles can be indexed to the tetragonal structure (JCPDS card 07-0209) with well-defined (112), (004), (200), (204), (220), (116), (312), (224), and (316) diffraction peaks. The XRD peaks for all the samples are broad, which indicates the nanocrystallinity of the samples.

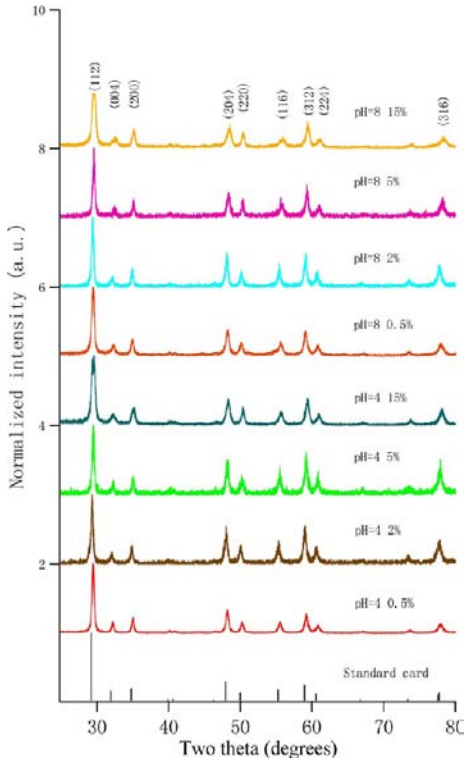

Figure 1. XRD patterns of $CdMoO_4$:Mn (0.5%, 2%, 5%, 15%) prepared at different pH values (pH = 4, pH = 8) in comparison to the standard JCPDS card for the tetragonal phase of $CdMoO_4$ (JCPDS 07-0209).

Figure 2 shows representative FESEM images and size distribution of the as synthesized $CdMoO_4$:Mn nanocrystals. The low temperature synthesis at pH = 4 produces spherical nanocrystals with a tail in the distribution toward larger particles (Figure.2 insets). The distribution was obtained with measurements over 150 nanoparticles. The average crystal size for Mn doping concentration of 0.5%, 2%, 5%, and 15% is 35, 41, 43, and 55 nm, respectively. The size increases with the Mn concentration. The dopant effect on crystal size has also been observed in other materials, ZnO:Al,[20] Al_2O_3-doped MnO, CdO, MoO,[21] and ZnS:Cu.[22] It is possible the size of $CdMoO_4$:Mn increases with the Mn concentration due to the presence of stress induced by the difference in the ionic radius between Cd^{2+} (R = 0.095 nm) and Mn^{2+} (R = 0.08 nm).[20] Liu et al. invoked a mechanism based on the effect of dopant on the crystal growth rate through surface charge modification,[17] which leads to variation of the size of the nanocrystals in Gd-doped $NaYF_4$ nanocrystals. A plot of the diameter of the $CdMoO_4$:Mn nanocrystals versus Mn doping concentration (Figure 3) shows a linear correlation between the two: $d = A + BC_{Mn}$ where d (nm) is the diameter of the nanocrystals, C_{Mn} is the Mn concentration, A(nm) is the diameter of $CdMoO_4$ without Mn doping. B is a positive constant. By fitting, the parameters A (nm) and B were found to be 36.4 (nm) and 1.3 (nm/%). So the relationship between the $CdMoO_4$:Mn diameter and Mn concentration can be expressed as $d = 36.4 + 1.3C_{Mn}$. Using this formula, the diameter of the $CdMoO_4$:Mn samples can be obtained approximately.

dx.doi.org/10.1021/ic3006663 | Inorg. Chem. 2012, 51, 9232−9239

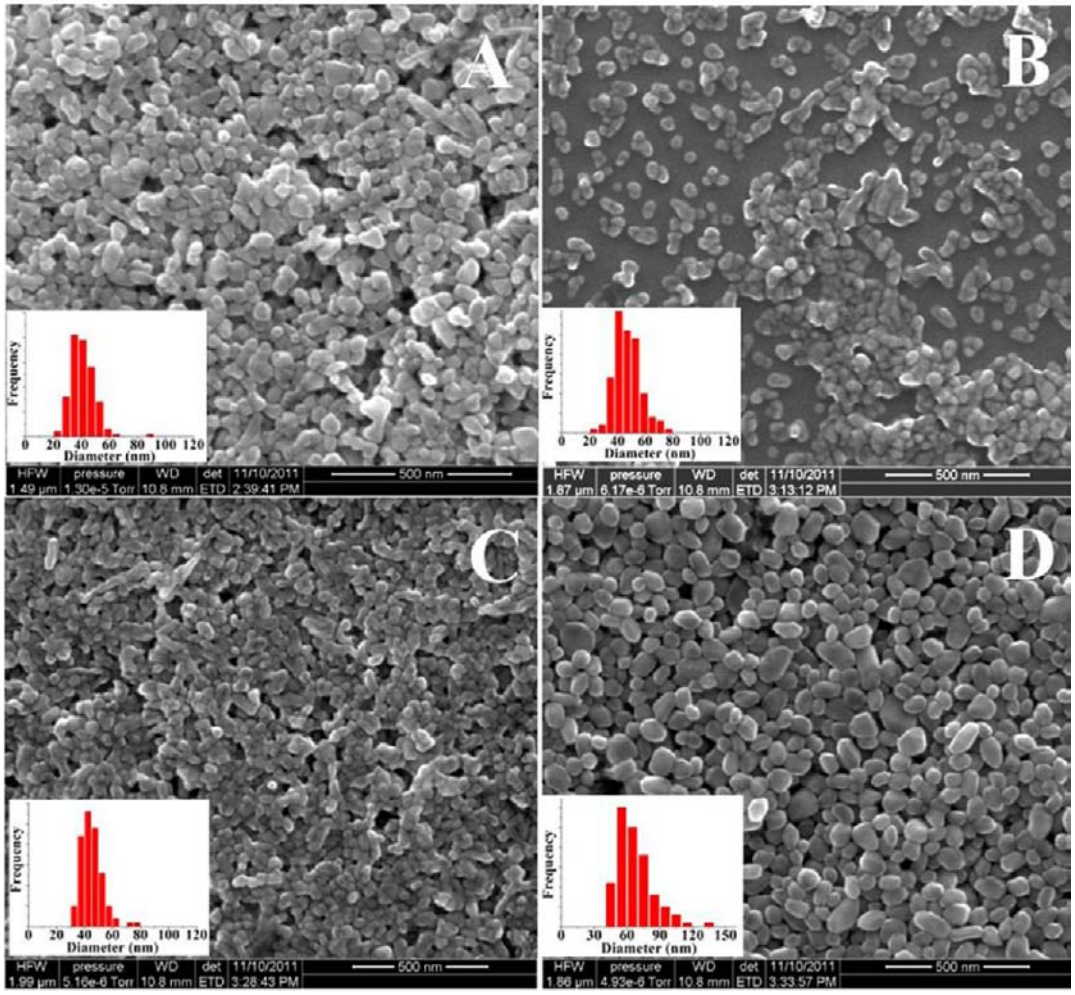

Figure 2. FESEM images of $CdMoO_4$:Mn nanocrystals prepared at pH = 4 with different Mn doping concentration A: 0.5%, B: 2%, C: 5%, D: 15% (all the scale bars are 500 nm). Insets show corresponding size distribution.

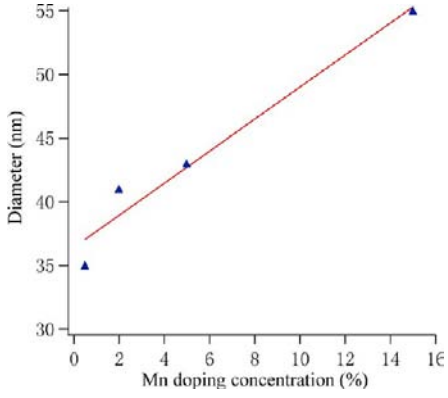

Figure 3. Dependence of the diameter of the $CdMoO_4$:Mn nanocrystals on Mn doping concentration; scattered dots are experimental data, and the solid line is the fit to the experimental data.

Figure 4 shows the FESEM images of $CdMoO_4$:Mn nanocrystals prepared at pH = 8 with different amount of Mn. The low temperature synthesis of $CdMoO_4$:Mn (0.5% Mn) produces nanocrystals of about 55 nm (Figure 4A) at pH = 8. When the Mn concentration is 2%, the corresponding average size is about 0.5 μm (Figure 4B) with a spherical morphology consisting of smaller nanoparticles. Tire-shaped microparticles (Figure 4C) of about 4 μm were obtained as the Mn concentration was increased to 5%. Doping 15% Mn in the low temperature synthesis leads to 8.5 μm spherical microparticles. The $CdMoO_4$:Mn microparticles at higher Mn concentrations (5%, 15%) in E and F of Figure 4 are formed by smaller nanoparticles which is similar to $CdMoO_4$:Mn (2% Mn) (Figure 4B). The size of the microparticles increases with increasing Mn concentration. The $CdMoO_4$:Mn microparticles are composed of aggregated smaller nanoparticles when the Mn concentration is higher than 2%. There are two growth stages during the low temperature synthesis of $CdMoO_4$:Mn at pH =8 when the Mn doping level is higher than 2%, according to the growth mechanism proposed by Wang et al. in template-free fabrication of $CdMoO_4$ hollow spheres.[10] One refers to the growth of the $CdMoO_4$:Mn nanoparticles, in which tiny $CdMoO_4$ nanoparticles were quickly produced when MoO_4^{2-} was added to the solution containing Cd^{2+} and spontaneously form large spheres to minimize their surface energy. The other is the formation of aggregated $CdMoO_4$:Mn microstructures through Ostwald ripening, in which large crystallites grow at the expense of small ones through the diffusion of ions, atoms, or molecules. The growth mechanism is strongly dependent on the pH and Mn doping concentration in low temperature growth. The $CdMoO_4$:Mn nanocrystals prepared at pH = 4 experience only the first stage during the growth. Ostwald ripening responsible for the $CdMoO_4$:Mn microstructure only

dx.doi.org/10.1021/ic3006663 | Inorg. Chem. 2012, 51, 9232–9239

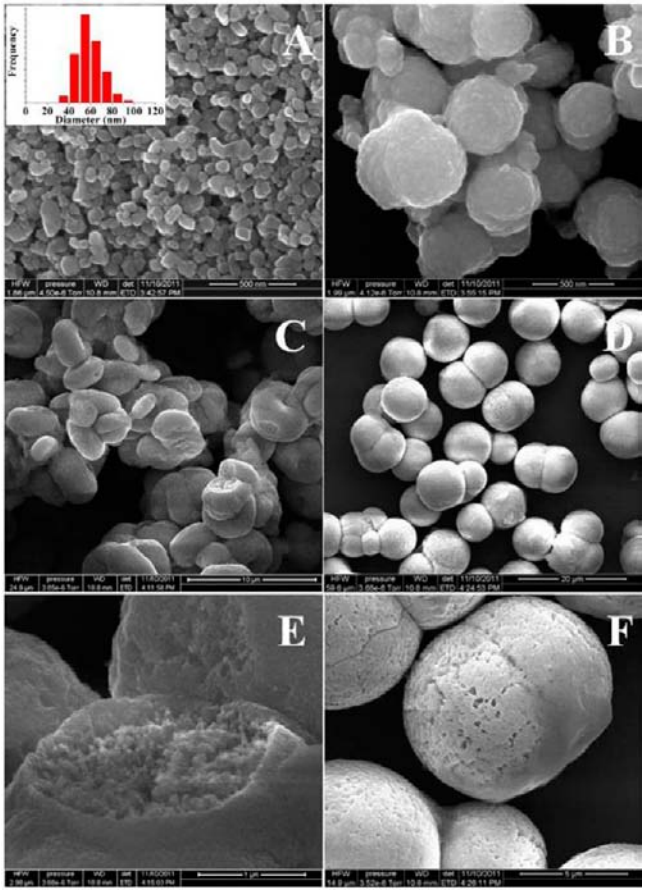

Figure 4. FESEM images of $CdMoO_4$:Mn prepared at pH = 8 with different Mn doping concentration. A: 0.5%, B: 2%, C: 5%, D: 15%. E and F are selected areas of C and D, respectively, at higher magnification. The inset of A is the size distribution measured over 100 particles. The scale bars are 500 nm, 500 nm, 10 μm, 20 μm, 1 μm, and 5 μm for A, B, C, D, E and F, respectively.

happens at higher Mn concentration when the solution is in basic environment.

3.2. UV–Vis Absorption Spectra. The solution-phase optical absorption spectra in deionized water for the $CdMoO_4$:Mn prepared at pH = 4 with different Mn doping concentration are shown in Figure 5. The absorption band observed at 230 nm and 300 nm are assignable to the molybdate group absorption. The two absorption band feature has been observed previously in the absorption spectra of $CdMoO_4$ nanoparticles made by microwave-assisted method.[23] The band gap of $CdMoO_4$:Mn nanocrystals synthesized by the low-temperature method can be evaluated by the absorption edge as shown in Figure 5. The band gaps are 4.47, 4.60, 4.73, and 4.78 eV for 0.5%, 2%, 5%, and 15% samples, respectively.

4. LUMINESCENCE PROPERTIES

The luminescence of tungstates and molybdates has the similar origin. All of them originate from two parts: one is from the intrinsic structure—the charge transfer from excited 2p orbits of O^{2-} to the empty orbits of the central Mo^{6+} ions, and the other is from the structural defects. There are only a few report about these kinds of defects; some authors ascribe that to the transitions in a tungstate or molybdate group, which lack one oxygen ion.[14,24] The room temperature photoluminescence spectra (PL) λ_{ex} = 325 nm and photoluminescence excitation

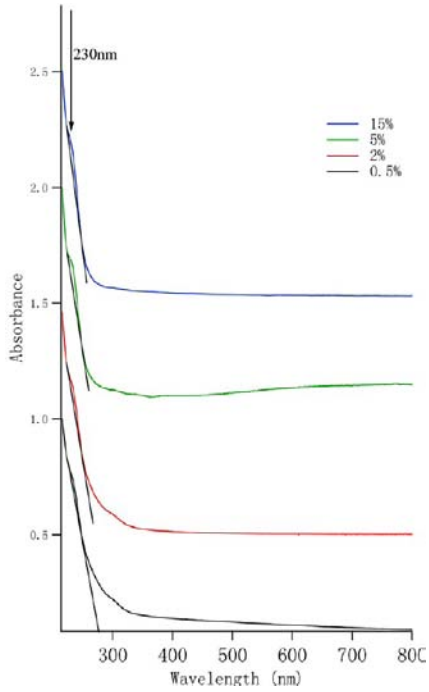

Figure 5. Absorption spectra of $CdMoO_4$:Mn nanocrystals prepared at pH = 4 with different Mn doping concentrations.

spectra (PLE) monitored at 510 nm (pH = 4) and 530 nm (pH = 8) for the $CdMoO_4$:Mn (5%) nanocrystals are shown in Figure 6. The PLE (Figure 6, left) of the two samples with

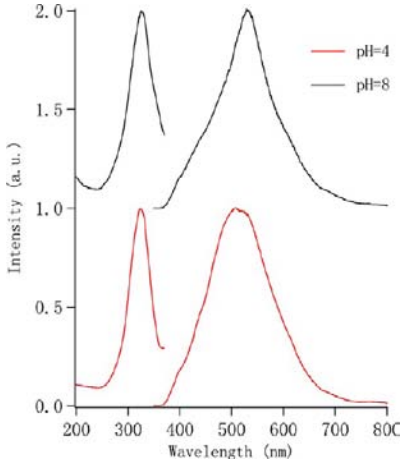

Figure 6. Room temperature photoluminescence excitation spectra (PLE) and photoluminescence spectra (PL) of $CdMoO_4$:Mn (5%) nanocrystals λ_{ex} = 325 nm (pH = 4 and 8). λ_{em} = 510 nm (pH = 4) and λ_{em} = 530 nm (pH = 8).

different pH look identical featuring the 325 nm excitation band between 250 and 360 nm assignable to the lowest exciton absorption band originating from the allowed optical transition from the O 2p state to the hybridized Mo 4d–Cd 5s state.[25] A broad PL spectra of the pH = 4 and pH = 8 samples centered at 510 nm and 530 nm (range 365–800 nm) originates from its intrinsic structure (the charge transfer from excited 2p orbits of O^{2-} to the empty orbits of the central Mo^{6+} ions[26–28]), and structural defects is observed as shown in Figure 6, right. The PL spectra of the pH = 8 sample is not as symmetrical as that of the pH = 4 sample, which is attributed to the different

dx.doi.org/10.1021/ic3006663 | Inorg. Chem. 2012, 51, 9232–9239

structural defects caused by different pH values during the synthesis. Similar results were reported for $CdWO_4$ nanocrystals.[14] The structure and defects, as well as the type and number of surface defects, depend on the pH value, leading to different photoluminescence properties.[14] Luminescence spectra of $CdMoO_4$:Mn (5%) nanocrystals (pH = 4 and pH = 8) measured at different temperatures from 77 to 300 K under the excitation of 325 nm are shown in Figure 7. The luminescence

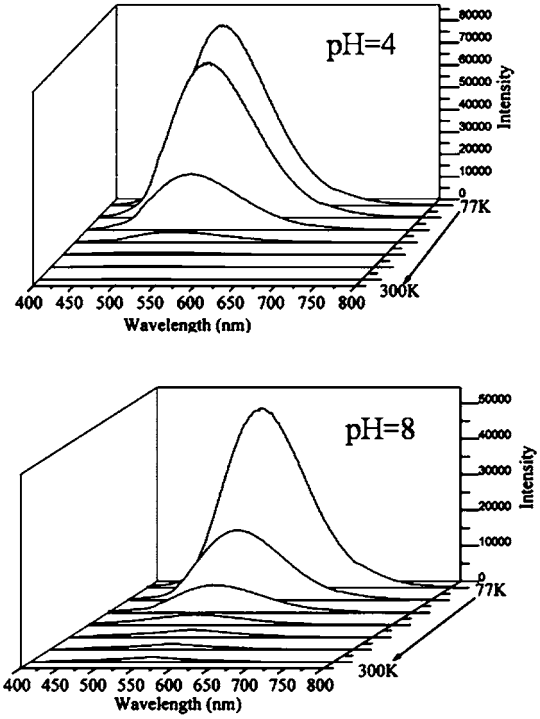

Figure 7. Photoluminescence spectra measured at different temperatures from 77 to 300 K excited at 325 nm for $CdMoO_4$:Mn (5%) pH = 4 and pH = 8.

intensity for both samples decreases dramatically as the temperature is increased from 77 to 300 K due to the temperature quenching effect.[29] The emission spectra shifted from 540 nm to 510 nm for pH = 4 sample, and shifted from 550 nm to 530 nm for the pH = 8 sample (Figure 7) when the temperature is increased from 77 to 300 K. That is caused by a redistribution of the emission originated from an overlap of the excitation edge of the intrinsic emission with the nearby absorption band of the defect centers.[28,30] The luminescence of Mn^{2+} would contribute to the visible range in certain wavelengths depending on the host matrix and would be much stronger at low temperature. However, the shape of the photoluminescence spectra for $CdMoO_4$:Mn (5%) is almost the same at different temperatures indicating that the Mn^{2+} luminescence is not strong enough to be observed even at low temperatures. Figure 8 shows the temperature dependence of the emission intensity of $CdMoO_4$:Mn (5%) (pH = 4 and pH = 8). The intensity as a function of temperature is well fitted by the well-known thermal activation function.[31]

$$I = \frac{I_0}{1 + \alpha\, e^{-E_A/k_B T}}$$

where I_0 is the emission intensity at 0 K, α is the proportionality coefficient, E_A is the thermal activation energy, k_B is Boltzmann's constant, and T is the absolute temperature. The

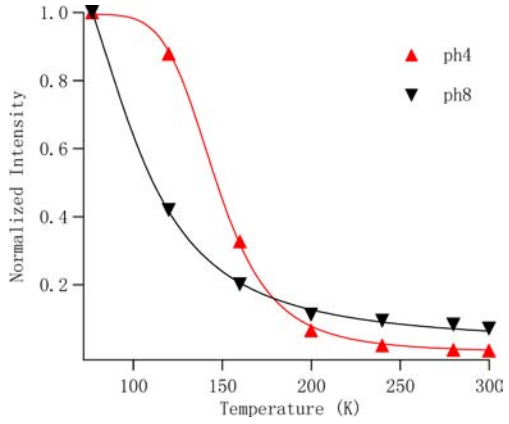

Figure 8. Dependence of emission intensity on temperature for $CdMoO_4$:Mn (5%) pH = 4 and pH = 8 samples.

values of I_0, α, and E_A obtained by fitting are listed in Table 1. E_A for pH = 4 is 117.5 meV which is almost three times that of the pH = 8 sample (38.2 meV).

Table 1. Fitting Parameters I_0, α, and E_A According to Thermal Activation Function

	pH = 4	pH = 8
I_0	0.99 + 0.01	1.26 + 0.05
α	10852.98 + 3178	82.16 + 9.17
E_A (meV)	117.5 + 0.4	38.2 + 0.2

It suggests that, for the luminescence of $CdMoO_4$:Mn (5%) nanocrystals, the pH = 4 sample is more thermally stable than the pH = 8 sample. More OH and carbonate groups could be absorbed on the nanocrystal surfaces in the preparation for the pH = 8 sample.[14] These groups with large vibrational energy may act as quenching centers,[32,33] leading to increased nonradiative relaxation rate and decreased E_A. Thus the pH = 4 sample has a higher thermal activation energy compared to that of the pH = 8 sample. The E_A for $CdMoO_4$:Mn nanocrystals is smaller than that of undoped $CdMoO_4$ single crystal (0.25 eV)[25] which is attributed to the influence of the defects in $CdMoO_4$:Mn nanocrystals prepared by low-temperature method.[34]

5. MAGNETIC PROPERTIES

In Figure 9, the pH and Mn concentration-dependent magnetic susceptibility (χ) versus temperature (T) plots for $CdMoO_4$:Mn are shown (cooled in zero field).The susceptibility is plotted in the unit of emu/mol Oe of $CdMoO_4$ nanocrystals. The applied magnetic field in each case is 500 Oe. All samples show similar features. A rapid increase in the magnetic susceptibility is observed below 50 K, exhibiting classical paramagnetic behavior (PM) caused by Mn local moments. The signal-to-noise ratio is quite small for 0.5% Mn doping of both pH = 4 and pH = 8 samples due to the small amount of Mn in the two. The inverse of the magnetic susceptibility of the samples are shown in Figure 10. Samples exhibit Curie–Weiss behavior plus a temperature-independent susceptibility term, χ_0. The inverse of the susceptibility follows $1/\chi = 1/(C/(T - \theta) + \chi_0)$ (C is the Curie constant, T is temperature in Kelvin, θ is the paramagnetic Curie temperature, and χ_0 is the temperature-independent term). The Curie–Weiss behavior dominates in samples with higher Mn

dx.doi.org/10.1021/ic3006663 | Inorg. Chem. 2012, 51, 9232–9239

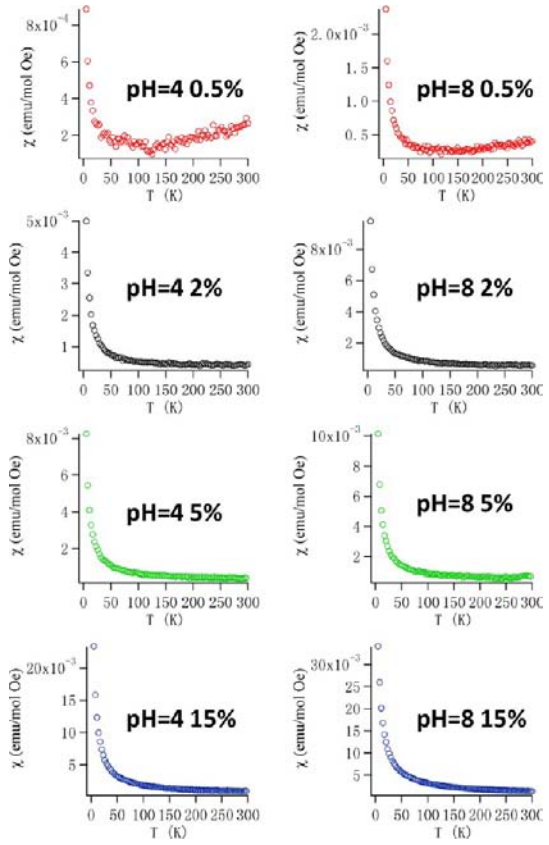

Figure 9. Temperature-dependent magnetic susceptibility of $CdMoO_4$:Mn prepared at pH = 4 and pH = 8 with different doping concentrations.

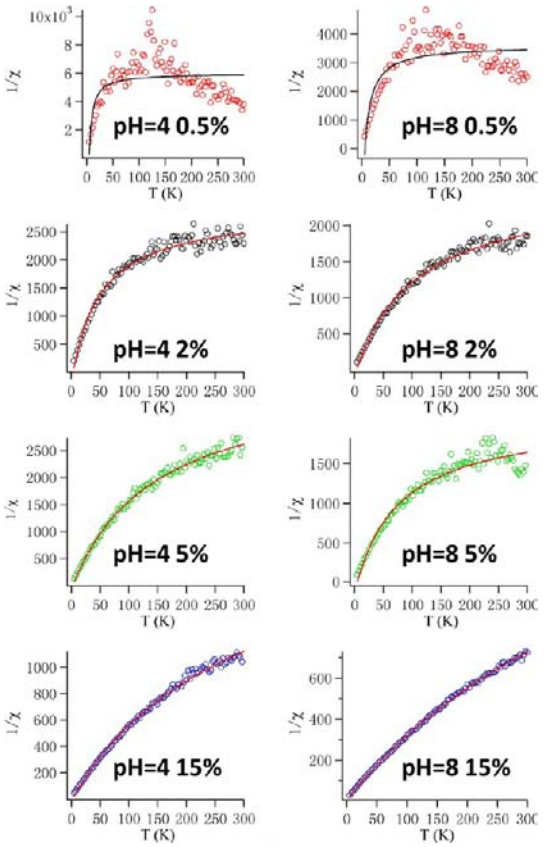

Figure 10. pH- and Mn concentration-dependent Curie–Weiss behavior for $CdMoO_4$:Mn.

concentrations, especially for the two 15% samples prepared at pH = 4 and pH = 8. The decrease in $1/\chi$ at high temperatures (and the poor fit) for the samples with the lowest Mn concentration (0.5%) is due to a slightly temperature-dependent diamagnetic signal of the base compound $CdMoO_4$. The magnetic susceptibilities of undoped $CdMoO_4$ samples prepared with the same methods were measured and show negative χ with decreasing magnitude at high temperature, which is the reason for the upturn in χ (decrease in $1/\chi$) seen in the 0.5% samples. Fits to the data using the above equation were performed over the entire experiment temperature range. Results show positive χ_0 for all doped samples (see Table 2). The paramagnetic Curie temperature θ is positive, except for one sample, indicative of ferromagnetic coupling between the Mn moments in the $CdMoO_4$:Mn lattice, although ferromagnetic ordering can be ruled out over the temperatures observed. θ decreases with increasing Mn concentration and changes sign for the pH = 8 (15%) sample, indicating weak antiferromagnetic (AFM) exchange interactions between the Mn moments at high concentrations. The positive θ value for the pH = 4 (15%) sample suggests the transition to AFM exchange interaction is hindered to some extent due to the nanoparticle nature of the sample.

EPR, which is a sensitive probe of the ground-state electronic structure of Mn^{2+}, was performed. Figure 11 shows the EPR spectra recorded at room temperature for the eight $CdMoO_4$:Mn samples. The EPR spectra exhibit resonance lines with a well-resolved hyperfine splitting of the central Mn^{2+} sextet for the samples with lower Mn concentrations. More hyperfine splitting is observed and is characterized as the forbidden doublet associated with axial symmetry.[35,36] The double peaks are most clearly seen in the pH = 8 (0.5%) sample, although they are also apparent in other samples. Sample pH = 4 (0.5%) exhibits a combined single peak, which is due to the small sizes of the nanocrystals.[37] As the Mn concentration increases to 5%, the peaks of the hyperfine sextet broaden due to the dipole–dipole interaction between the Mn^{2+} moments. The EPR spectrum evolves to a singlet with incomplete sextet superimposed for the $CdMoO_4$ samples with the highest Mn concentration (15%). The line width increase and evolution of the EPR spectra with the Mn concentration are consistent with the increasing dipole–dipole interaction as the doping level changes from 0.5% to 15%. The spin Hamiltonian parameters (g, A, and D values) listed in Table 3 can be obtained by fitting the spectra to a spin Hamiltonian.[38]

$$\hat{H} = g\beta H\cdot S + AS\cdot I + D\left[S_z^2 - \frac{1}{3}S(S+1)\right]$$

where H is the Zeeman field, g is the Lande g factor, β is the Bohr magneton, A is hyperfine constant, S and I are the electron and nuclear spin operators, and D is the zero-field splitting. The fitted g values from Figure 11 are close to 1.987, which is typical for Mn(II) ions.[38–40] The absolute hyperfine constants (A) are in the range of 87.2–88.1 × 10^{-4} cm^{-1}, which are in very good agreement with the reported values for Mn (II)-doped single-crystal $CdMoO_4$[41]. The similar spin Hamiltonian parameters obtained indicate successful Mn(II) doping in the nanocrystals.[38] The zero-field splitting (D) term is in the range of 51–68 × 10^{-4} cm^{-1}. Compared to that for single crystal (~30 × 10^{-4} cm^{-1}),[41] the larger D value can be

dx.doi.org/10.1021/ic3006663 | Inorg. Chem. 2012, 51, 9232–9239

Table 2. Parameters C, θ, and χ_0 Obtained from the Fitting

	pH = 4				pH = 8			
Mn	0.5%	2%	5%	15%	0.5%	2%	5%	15%
C	0.001	0.02	0.04	0.13	0.003	0.04	0.04	0.27
θ	4.73	3.62	2.38	1.83	5.67	4.03	3.68	−1.96
$\chi_0(10^{-4})$	1.67	3.4	2.56	4.5	2.78	3.9	4.3	4.73

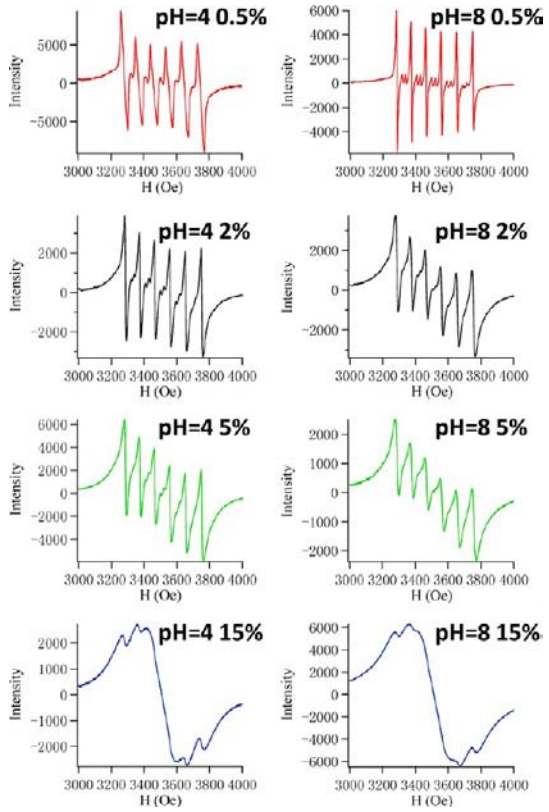

Figure 11. EPR spectra showing pH and Mn concentration dependence for $CdMoO_4$:Mn.

Table 3. Spin Hamiltonian Parameters of $CdMoO_4$:Mn Nanocrystals

samples	g	A (10^{-4} cm^{-1})	D (10^{-4} cm^{-1})
pH = 4, Mn 0.5%	1.9879	−87.5	51.4
pH = 4, Mn 2%	1.9864	−87.4	55.1
pH = 4, Mn 5%	1.9868	−87.3	59.5
pH = 4, Mn 15%	1.9863	−87.6	54.0
pH = 8, Mn 0.5%	1.9865	−87.3	54.3
pH = 8, Mn 2%	1.9867	−87.2	63.2
pH = 8, Mn 5%	1.9863	−87.7	67.4
pH = 8, Mn 15%	1.9867	−88.1	59.9

understood in terms of larger lattice distortion in nanoparticles than in bulk lattice.[38]

6. CONCLUSIONS

A low-temperature (2 °C) aqueous coprecipitation method has been developed to prepare $CdMoO_4$:Mn nanocrystals. The crystal size increases linearly with increasing Mn doping concentration for pH = 4, which is caused by the dopant-induced effect on the crystal growth rate. Lower pH and lower Mn doping concentration prohibit the Ostwald process during the growth, result in uniform nanospheres of narrow size distribution, and avoid aggregated $CdMoO_4$:Mn microstructures, which lead to higher luminescence thermal stability. The strength of the ferromagnetic exchange coupling between Mn moments decreases with increasing Mn concentration, and it changes sign to an antiferromagnetic one for the pH = 8 (15%) sample. The coupling remains positive for the pH = 4 (15%) sample most likely because its small particle size hinders the transition to the antiferromagnetic coupling at such high concentrations. EPR spectra show evolution from well-resolved hyperfine splitting of the Mn^{2+} central sextet at low Mn concentration to a singlet at high concentration. The spin Hamiltonian parameters obtained by fitting indicate successful Mn(II) doping in the nanocrystals.

AUTHOR INFORMATION

Corresponding Author

*E-mail: jtang2@uwyo.edu

Notes

The authors declare no competing financial interest.

ACKNOWLEDGMENTS

This work was supported by the U.S. Department of Energy, Office of Basic Energy Sciences, Division of Materials Sciences and Engineering under Award DE-FG02-10ER46728. We thank Dr. Leonard Spinu and Mr. Shankar Khanal at the University of New Orleans for their kind assistance on EPR measurements. We also thank Dr. Weiwei Zheng at Emory University and Dr. R. V. S. S. N. Ravikumar at Acharya Nagarjuna University for the calculations and discussions of spin Hamiltonian parameters.

REFERENCES

(1) Liao, H. W.; Wang, Y. F.; Liu, X. M. *Chem. Mater.* **2000**, *12*, 2819−2821.
(2) Wang, H.; Medina, F.; Liu, D. *Phys. Rev. B.* **1992**, *45*, 10356−10362.
(3) Errandoneaa, D.; Kumar, R. S.; Ma, X. H. *J. Solid State Chem.* **2008**, *181*, 355−364.
(4) Qi, T.; Takagi, K.; Fukazawa, T. *Appl. Phys. Lett.* **1980**, *36*, 278−279.
(5) Mikhailik, V. B.; Kraus, H.; Wahl, D. *Phys. Status Solidi B* **2005**, *242*, R17−R19.
(6) Jayaraman, A.; Wang, S. Y.; Sharma, S. K. *Phys. Rev. B.* **1995**, *52*, 9886−9889.
(7) Beckmann, P. A.; Bai, S.; Dybowski, C. *Phys. Rev. B.* **2005**, *71*, 12410−12411.
(8) Jiang, X.; Ma, J.; Lin, B.; Ren, Y.; Liu, J.; Zhu, X.; Tao, J. *J. Am. Ceram. Soc.* **2007**, *90*, 977−979.
(9) Gong, Q.; Li, G.; Qian, X.; Cao, H.; Du, W.; Ma, X. D. *J. Colloid Interface Sci.* **2006**, *304*, 408−412.
(10) Wang, W. S.; Zhen, L.; Xu, C. Y.; Zhang, B. Y.; Shao, W. Z. *J. Phys. Chem. B* **2006**, *110*, 23154−23158.
(11) Kawasaki, H.; Hamaguchi, K.; Osaka, I.; Arakawa, R. *Adv. Funct. Mater.* **2011**, *21*, 3508−3515.
(12) Rim, H. P.; Min, K. H.; Lee, H. J.; Jeong, S. Y.; Lee, S. C. *Angew. Chem.* **2011**, *123*, 9015−9019.

(13) Yu, L. X.; Song, H. W.; Lu, S. Z.; Liu, Z. G.; Yang, L. M.; Kong, X. G. *J. Phys. Chem. B.* **2004**, *108*, 16697−16702.
(14) Dai, Q. L.; Song, H. W.; Pan, G. H.; Bai, X.; Zhang, H.; Qin, R. F.; Hu, L. Y.; Zhao, H. F.; Lu, S Z.; Ren, X. G. *J. Appl. Phys.* **2007**, *102*, 054311.
(15) Ida, S.; Ogata, C.; Matsumoto, Y. *J. Phys. Chem. C* **2009**, *113*, 1896−1900.
(16) Bai, X.; Song, H. W.; Yu, L. X.; Yang, L. M.; Liu, Z. X.; Pan, G. H.; Lu, S. Z.; Ren, X. G.; Lei, Y. Q.; Fan, L. B. *J. Phys. Chem. B* **2005**, *109*, 15236−15242.
(17) Wang, F.; Han, Y.; Lim, C.; Lu, Y.; Wang, J.; Xu, J.; Chen, H.; Zhang, C.; Hong, M.; Liu, X. *Nature* **2010**, *463*, 1061−1065.
(18) Chen, D.; Yu, Y.; Huang, F.; Huang, P.; Yang, A.; Wang, Y. *J. Am. Chem. Soc.* **2010**, *132*, 9976−9978.
(19) Tian, G.; Gu, Z.; Zhou, L.; Yin, W.; Liu, X.; Yan, L.; Jin, S.; Ren, W.; Xing, G.; Li, S.; Zhao, Y. *Adv. Mater.* **2012**, *24*, 1226−1231.
(20) Lee, J. H.; Park, B. O. *Mater. Sci. Eng., B* **2004**, *106*, 242−245.
(21) Farag, I. S. A.; Battisha, I. K.; El-Rafaay, M. M. *Indian J. Pure Appl. Phys.* **2005**, *43*, 446−458.
(22) Wang, M.; Sun, L.; Fu, X.; Liao, C.; Yan, C. *Solid State Commun.* **2000**, *115*, 493−496.
(23) Phuruangrat, A.; Ekthammathat, N.; Thongtem, T.; Thongtem, S. *J. Phys. Chem. Solids* **2011**, *72*, 176−180.
(24) Lammers, M. J. J; Blasse, G.; Robertson, D. S. *Phys. Status Solidi A* **1981**, *63*, 569−572.
(25) Itoh, M. *J. Lumin.* **2012**, *132*, 645−651.
(26) Blasse, G. *Struct. Bonding (Berlin)* **1980**, *42*, 1−41.
(27) Li, Y. F.; Mi, Y.; Jiang, J. Y.; Huang, Z. Y. *Chem. Lett.* **2010**, *39*, 760−761.
(28) Itoh, M.; Sakurai, T. *Phys. Rev. B* **2006**, *73*, 235106.
(29) Coffa, S.; Franzo, G.; Priolo, F.; Polman, A.; Serna, R. *Phys. Rev. B* **1994**, *49*, 16313−16320.
(30) Mikhailik, V. B.; Kraus, H.; Wahl, D.; Itoh, M.; Koike, M.; Bailiff, I. K. *Phys. Rev. B* **2004**, *69*, 205110.
(31) Li, B.; Liu, Y.; Zhi, Z.; Shen, D.; Lu, Y.; Zhang, J.; Fan, X. *J. Cryst. Growth* **2002**, *240*, 479−483.
(32) Yu, H. Q.; Song, H. W.; Pan, G. H.; Fan, L.; Li, S.; Bai, X.; Zhao, H. *J. Lumin.* **2007**, *124*, 39−44.
(33) Bai, X.; Song, H. W.; Pan, G. H.; Liu, Z. X; Lu, S. Z.; Di, W. H.; Ren, X. G.; Lei, Y. Q.; Dai, Q. L.; Fan, L. B. *Appl. Phys. Lett.* **2006**, *88*, 143104.
(34) Peng, H.; Song, H.; Chen, B.; Wang, J.; Lu, S.; Kong, X.; Zhang, J. *J. Chem. Phys.* **2003**, *118*, 3277−3282.
(35) Mazur, M.; Kleinova, M.; Moncol, J.; Stachova, P.; Valko, M.; Telser, J. *J. Non-Cryst. Solids* **2006**, *352*, 3158−3165.
(36) Dewijn, H. W.; Vanbalde, Rf. *J. Chem. Phys.* **1967**, *46*, 1381−1387.
(37) Bottcher, R.; Klimm, C.; Michel, D.; Semmelhack, H.-C.; Volkel, G.; Glasel, H.-J.; Hartmann, E. *Phys. Rev. B* **2000**, *62*, 2085−2095.
(38) Zheng, W.; Wang, Z.; Wright, J.; Goundie, B.; Dalal, N. S.; Meulenberg, R. W.; Strouse, G. F. *J. Phys. Chem. C* **2011**, *115*, 23305−23314.
(39) Wang, Z.; Zheng, W.; van Tol, J.; Dalal, N. S.; Strouse, G. F. *Chem. Phys. Lett.* **2012**, *524*, 73−77.
(40) Zheng, W.; Wang, Z.; van Tol, J.; Dalal, N. S.; Strouse, G. F. *Nano Lett.* **2012**, *12*, 3132−3137.
(41) Biederbick, R.; Born, G.; Hofstaetter, A.; Scharmann, A. *Z. Phys. B* **1975**, *22*, 219−222.